Applied Nanoscience (2020) 10:1535–1544
https://doi.org/10.1007/s13204-019-01239-3

ORIGINAL ARTICLE

Enhanced industrial dye degradation using Co doped in chemically exfoliated MoS_2 nanosheets

Ali Raza[1,2] · Muhammad Ikram[2] · Muhammad Aqeel[2] · Muhammad Imran[3] · Anwar Ul-Hamid[4] · Khalid Nadeem Riaz[5] · Salamat Ali[1]

Received: 19 October 2019 / Accepted: 10 December 2019 / Published online: 18 December 2019

Abstract

Cobalt concentrations of 7.5 and 10 wt% were incorporated in chemically exfoliated molybdenum disulfide (MoS_2) nanosheets using hydrothermal route. Various characterization techniques were employed to evaluate the Co-doped MoS_2 for structural, physiochemical, optical, and morphological properties. X-ray diffraction (XRD) technique confirmed the increase in crystallinity and crystallite size with doping ratios. The presence of functional groups and vibrational characteristic peak of Mo–O was determined using Fourier-transform infrared spectroscopy (FTIR). Field emission scanning electron microscope (FESEM) and high-resolution transmission electron microscope (HR-TEM) micrographs showed surface morphology and interlayer spacing. Absorption spectra and bandgap energy decreased with conjugation of Co ascribed to quantum confinement and edge effects as investigated using UV–visible spectroscopy. Thermal properties of prepared samples depicted weight and thermal stability as confirmed by differential scanning calorimeter and thermogravimetric analysis (DSC-TGA). Photoluminescence (PL) spectra confirmed the presence of doped species and revealed the growth of MoS_2 monolayer. Dye degradation of doped and undoped MoS_2 was tested in the presence of catalyst sodium borohydride ($NaBH_4$) and it was observed that the methylene blue (MB) removal process increased with doping concentration. These nanocatalysts may prove useful in the removal of industrial contaminants, especially leather, and tanneries pollutants.

Keywords Doping · Co–MoS_2 · XRD · FESEM · HR-TEM · SAED · DSC-TGA · Nanosheet · Nanocatalysts

Introduction

Environmental pollution at a global level is generating serious issues including inadequate accessibility of desalinated water for a large segment of human population. Increase in population growth has reduced the access to clean water to around 750 million people only. A large part (97.5%) of global water is composed of salty water and only 2.5% fresh water is suitable for human consumption (Wang et al. 2018; Dervin et al. 2016). Water reservoirs are regularly contaminated by various hazardous pollutants such as organic chemicals. This persistent level of toxicity poses a substantial risk to living species and environment worldwide (Wu et al. 2018). Approximately, 1/10 million dyes are utilized annually in several sectors such as paper, leather, printing, textile etc. Among these dyes, mostly methylene blue (MB), 10–15% is directly released in water bodies, aquatic life, and atmosphere introduce serious diseases including cancer, skin irascibilities, and liver malfunctioning (Junaid et al. 2019).

Ali Raza and Muhammad Ikram are equal contributors.

✉ Muhammad Ikram
dr.muhammadikram@gcu.edu.pk

1 Department of Physics, Riphah Institute of Computing and Applied Sciences (RICAS), Riphah International University, 14 Ali Road, Lahore, Pakistan

2 Solar Cell Applications Research Lab, Department of Physics, Government College University Lahore, Punjab 54000, Pakistan

3 State Key Laboratory of Chemical Resource Engineering, Beijing Advanced Innovation Centre for Soft Matter Science and Engineering, Beijing Engineering Center for Hierarchical Catalysts, Beijing University of Chemical Technology, Beijing 100029, China

4 Center for Engineering Research, Research Institute, King Fahd University of Petroleum and Minerals, Dhahran 31261, Saudi Arabia

5 Department of Physics, University of Gujrat, HH Campus, Gujrat 50700, Pakistan

To remove salt and various contaminations from water appears relatively simple in theory, but to clean the water experimentally is highly challenging, extremely expensive, and time-consuming exercise (Dervin et al. 2016). Various techniques for elimination of contamination from industrial water and production of purified water have been deployed such as catalysis, electrolysis, photocatalysis, nano-adsorbents, ion exchange, carbon filter, disinfection and microbial control, membrane filtration, and reverse osmosis (RO) (Dervin et al. 2016; Junaid et al. 2019; Kunduru et al. 2017). Among these techniques, catalysis is environmental friendly, cost-effective, energy-efficient, and plays decisive role in degrading harmful pollutants efficiently (Junaid et al. 2019; Zhang 2018).

During the last few decades, semiconductor nanomaterials have generated a huge interest for researchers in the area of environmental development, as compared to existing water purification membrane materials. These nanomaterials have gained significance due to excellent physical and chemical properties, low toxicity, high electrochemical stability, finite size, and large surface area. Presently, 2D materials (molybdenum disulfide, boron nitride, graphene oxide, and tungsten disulfide) are emerging class that is being used to enhance the water desalination process. These materials exhibit exceptional mechanical, electronic, and optical properties (Dervin et al. 2016; Wahab et al. 2019; Yin 2014). Specifically, transition metal dichalcogenide MoS_2 exhibits inspiring physical and chemical properties and is known as a promising candidate for catalysis (Zhiming 2013; Mao et al. 2018).

So far, various efforts have been undertaken to enhance the catalytic performance of MoS_2 using doping, heterojunction, and noble metals (gold, silver, platinum, and iridium) depositions (Zhang 2018). In the present work, hydrothermal method was used to fabricate different ratios of Co-doped exfoliated MoS_2 nanosheets to evaluate its catalytic behavior.

Experimental details

Chemicals

Molybdenum disulfide (~ 6 µm, 99%) and hydrazine hydrate (N_2H_4) were acquired from "Sigma-Aldrich". Sodium nitrate ($NaNO_3$) and hydrochloric acid (37%) were procured from "Reagents Duksan" and "Analar", respectively. Cobalt acetate 4-hydrate, $Co(CH_3COO)_2.4H_2O$, was received from "Panreac". All the chemicals were used without additional purification.

MoS_2 exfoliation process

MoS_2 nanosheets were synthesized by chemical exfoliation method as shown in Fig. 1; $NaNO_3$ (6 g) was dissolved in 16 ml of concentrated HCl (37%) in one-neck round flask. Subsequently, bulk MoS_2 (1.2 g) was added and quenched with water. Prepared solution was ultrasonicated at 30 °C for 5 h with toxic gas collection setup. Furthermore, supernatant fraction was centrifuged at 6000 rpm for 30 min; eventually, grey-black precipitated MoS_2 nanosheets were collected (Lin 2017).

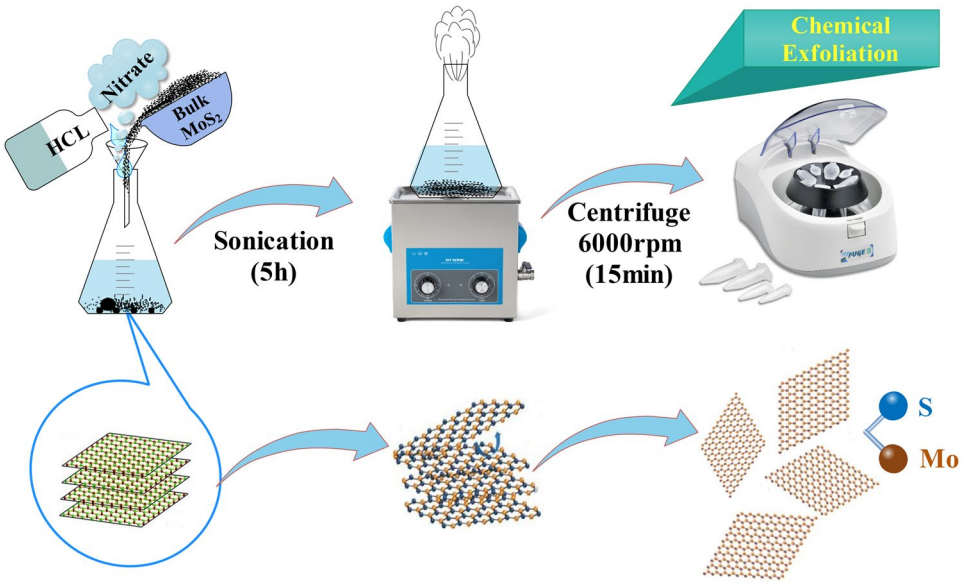

Fig. 1 Schematic diagram of MoS_2 exfoliation mechanism

Synthesis of Co-doped MoS_2 nanosheets

Hydrothermal route was used to synthesize different concentrations of Co to MoS_2 nanosheets as illustrated in Fig. 2, MoS_2 nanosheets (800 mg) were added in 80 ml water, 75–100 mg of $Co(CH_3COO)_2.4H_2O$ and 5 ml hydrazine hydrate were added under stirring at 70 °C for 15 min and subsequently transferred to tightly sealed 100 ml teflon-lined stainless steel autoclave. Reaction was carried out at 200 °C for 24 h, autoclave was cooled down to room temperature and the black solution was dried at 200–250 °C (Kumar et al. 2017).

Catalysis

Sodium borohydride ($NaBH_4$) solution was prepared by mixing 0.18 g sodium borohydride (SB) in 25 ml water. Freshly prepared SB solution (800 µL) was added to 3 ml aqueous MB. Then, 800 µL of doped MoS_2 nanosheets was incorporated under agitation. Decolorization of mixture indicates dye degradation which resulted in MB reduced to leucomethylene blue (LMB) in the presence of $NaBH_4$ as shown in Eq. 1. The nanocatalyst-free reaction was referred to as blank sample (Fig. 3); furthermore, absorption spectrum was monitored by UV–vis spectrophotometer at 200–800 nm in Fig. 9a–c (Naz et al. 2017).

Characterization

X-ray diffractometer (XRD) was employed to prepare Co-doped MoS_2 nanosheets by spectrum Bruker system (XRD, D2 Phaser, USA) equipped with monochromatized Cu Kα radiation of average wavelength 1.54059 Å with 2θ range 5–90° using scan rate 0.05/min. Fourier-transform infrared (FTIR) spectroscopy analysis was carried on Excalibur 3100 spectrometer with a spectral range of 4000–400 cm^{-1} by accumulation of 32 scans at resolution of 0.2 cm^{-1}, dry powdered nanoparticles were centrifuged for 15 min at 10,000 rpm; pellet was redirected to deionized water. Purified nanosheets were dried, and functional groups were examined in subsequent samples. Optical properties were investigated using UV–vis spectrophotometer (TECAN infinite M200PRO) used in the range of 275–400 nm. Morphology and microstructures of synthesized nanosheets were studied with field emission scanning electron microscope (FESEM), JSM-6460LV FESEM and inter layer distance detected by high-resolution transmission electron microscope (HR-TEM) Philips CM30 and JEOL 2000 FX. To confirm MoS_2 flakes, Raman spectra were recorded on Renishaw through reflex confocal Raman microscope with wavelength of 532 nm (6 mW) laser. Photoluminescence (PL) spectra of as prepared and

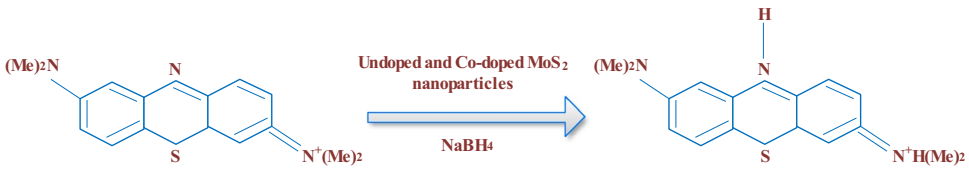

(1.)

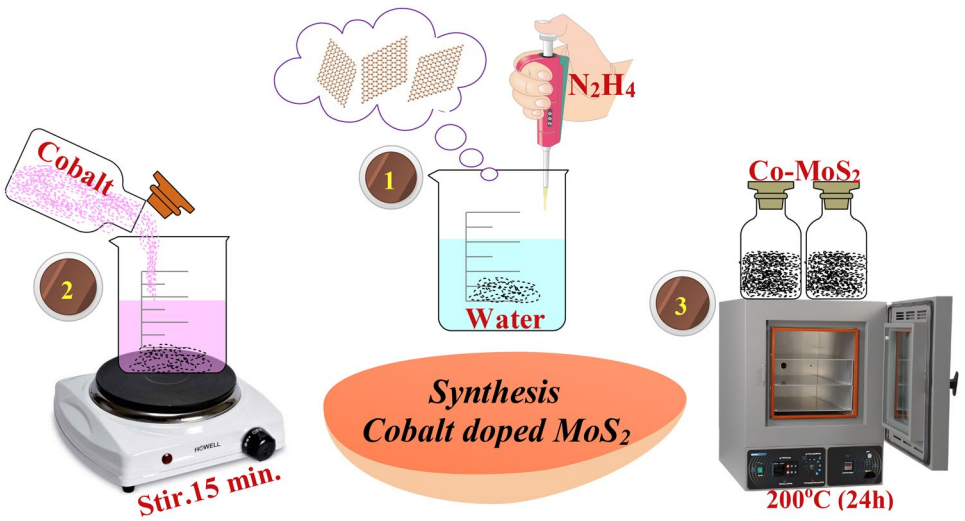

Fig. 2 Schematic diagram of Co-doped MoS_2 synthesis

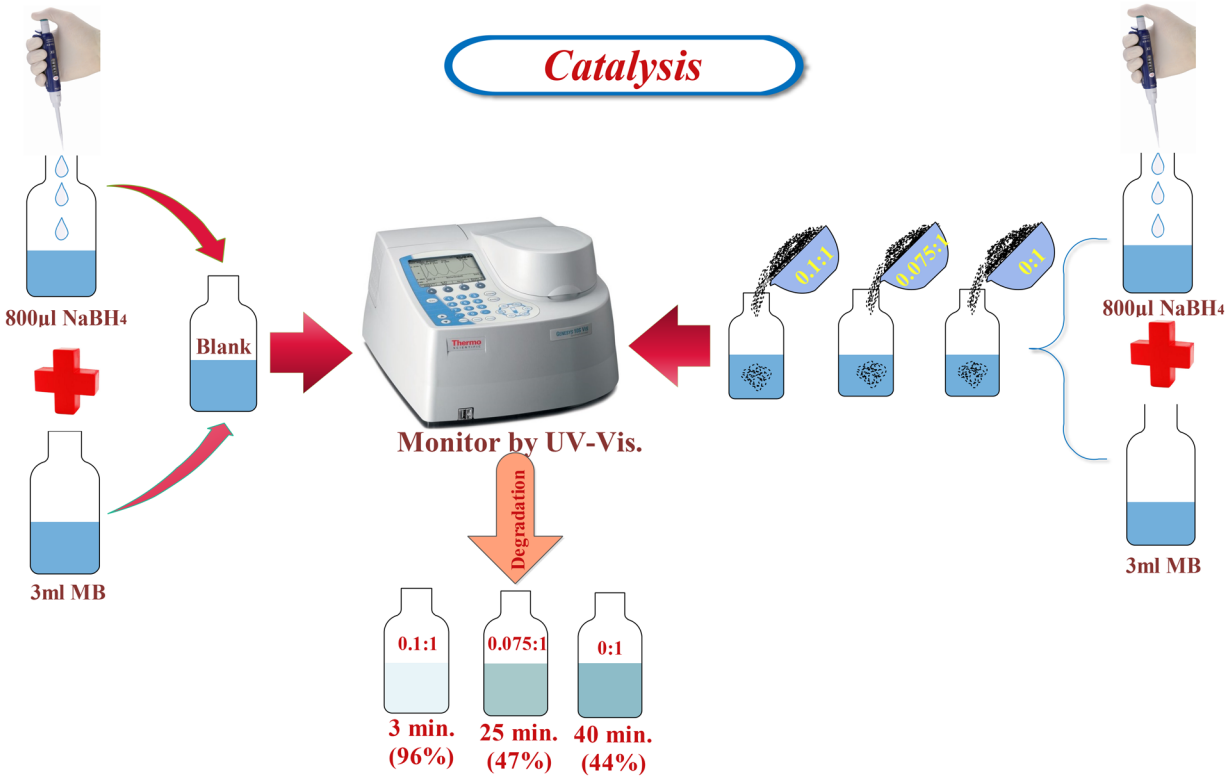

Fig. 3 Schematic diagram of synthesis and catalytic activity of Co-doped MoS_2

doped samples were recorded through spectrofluorometer (JASCO, FP − 8300).

Results and discussion

XRD was employed to determine the crystallite size and crystalline structure of prepared Co-doped MoS_2 nanosheets as shown in Fig. 4a. Observed patterns of undoped and Co-doped MoS_2 located reflections ~ 8.8°, 26.5°, 29.3°, 31.6°, 39.2°, 45.3°, 48.1°, 56.4°, 66.3°, 75.3°, and 84° are confirmed as (002), (420), (004), (100), (103), (006), (106), (106), (214), (116), and (− 117), respectively (Fig. 4a). These planes showed hexagonal structure of sheets without impurity and agree well with JCPDS cards No. 00-37-1492 and 01-081-2031 (66.3°, 84°) (Liu et al. 2014; Yi and Zhang 2018; Ma et al. 2016; Nethravathi et al. 2017). It is noteworthy that the peak (002) is observed with higher amount of doped Co (0.1:1) (Nethravathi et al. 2017; Li 2017). Low-intensity diffraction peaks specify low crystallinity of Co–MoS_2 and (004) face possibly resulted from partial restacking during the drying process (Li 2017; Ye et al. 2016). Significant peak (100) can be attributed to increase in crystallinity of nanosheets with incorporation of Co (Feng et al. 2015). Asymmetric 2D reflections around 57° reveal the existence of stacking defects within the few layers of Co–MoS_2 (Nethravathi et al. 2017). Average measured crystallite sizes were calculated using Scherer's formula, $D = \frac{k\lambda}{\beta\cos\theta}$ and were found to be in the range of ~ 16, 48.3, and 26.6 nm where $k = 0.89$ is constant, $\lambda = 0.154$ nm (wavelength of X-rays), β is broadening at full-width half maxima (FWHM) of peak in radian, and θ is corresponding to Bragg's diffraction angle in radian. These calculated crystallite sizes demonstrate an increase upon doping. The corresponding selected area electron diffraction (SAED) patterns of doped MoS_2 nanosheets are shown in Fig. 4b–d. The observed ring features confirm a polycrystalline MoS_2 in hexagonal structure, also providing evidence to the fact that the product is well crystallized; ring indexing is consistent with XRD results.

To elucidate chemical composition and bond identification present in product molecules, non-destructive FTIR technique was used (Fig. 4e) (Zeng et al. 2015; Singh 2019). Transmittance peaks from FTIR spectra are found around 841, 1380, 1636, 2427 and 3442 cm^{-1}, peaks ~ 841 and 1010 cm^{-1} indicating S–S characteristics stretching and S–O stretching respectively (Oudeng et al. 2018). Bands between 1100 and 1650 cm^{-1} are ascribed as stretching vibrations of hydroxyl (–OH) group adsorbed moisture during synthesis process and may be Mo–O

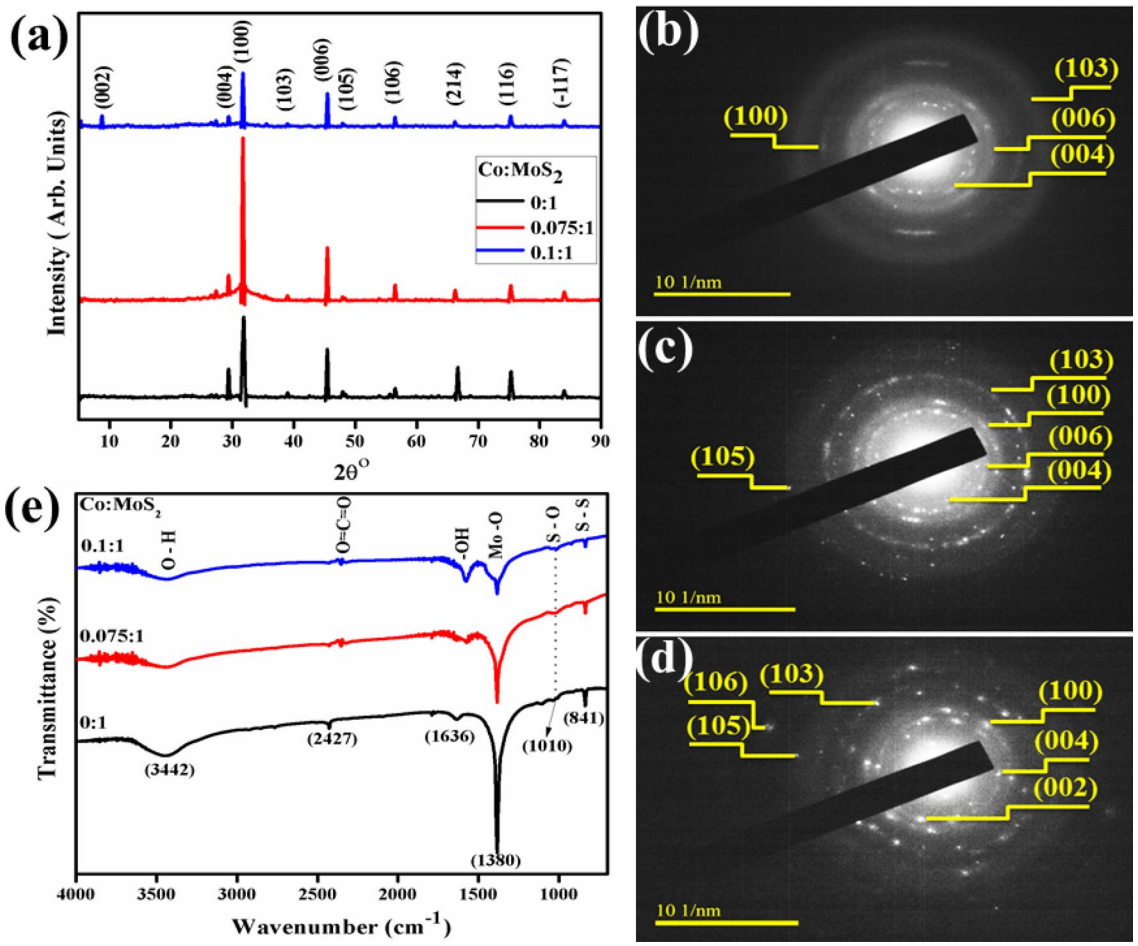

Fig. 4 **a** XRD pattern, **b–d** SAED pattern, **e** FTIR spectra of different ratios of Co to MoS_2

vibrations and C–N stretching (Vattikuti and Byon 2015; Wang 2016; Sim et al. 2017). Significant transmitted peak ~ 1380 cm^{-1} from spectra is confirmed as characteristic peak of νib(Mo–O) (Kumar et al. 2012; Wang et al. 2018). Broadband centered ~ 3500 cm^{-1} represents formation of symmetrical stretching vibration of O–H (Vattikuti and Byon 2015; Pineda-León et al. 2018). Peak observed around 2427 cm^{-1} showed presence of CO_2 in atmosphere during synthesis process (Wang et al. 2018).

Optical properties of doped materials using UV–vis spectrophotometer for absorbance spectra and bandgap (BG) analysis was studied in Fig. 5a, b. Absorption spectra displayed characteristic band between 275 and 320 nm provide evidence of absorption in UV zone (Vattikuti and Byon 2015; Peng 2015). With Co doping, absorption range increased towards longer wavelength can be attributed to quantum confinement and edge effects (Li 2017). To determine optical BG energies, Tauc transformation equation was used to draw graph between ($\alpha h\nu$) vs ($h\nu$) and by x-intercept of extrapolated linear fits (Junaid et al. 2019). However, introduction of Co reduced BG energies from 2.83 eV to 1.41 eV and 1.35 eV gradually (Vattikuti and Byon 2015; Peng 2015).

FESEM images 6(a, c, and e include inset) were supportive of revealed surface morphology and structure of synthesized samples. Undoped sample (Fig. 6a) showed non-uniform and aggregated morphology of nanosheets. Increased magnification is indicating a possibility of stacked layer existence that is a feature of MoS_2 structure (inset). Doped specimen image (Fig. 6c) exhibits high agglomeration of particles scattered over sheets. Upon higher doping (Fig. 6e), observed as chunk of MoS_2 layered structures; magnified area indicates layers compacted by Co-doped nanoparticles. High aggregation trend was observed upon Co doping relative to MoS_2 nanosheets. HR-TEM investigation in edge areas was a common and direct method to determine the layer numbers microscopically, HR-TEM images in Fig. 6b, d, f on a single grain depicts individual atomic planes ordered in the S–Mo–S sequence to form each layer and periodic atom arrangement of nanosheets at selected area, in which interplanar spacing was measured to be ~ 0.27 nm (Fig. 6b). According to the periodic pattern in

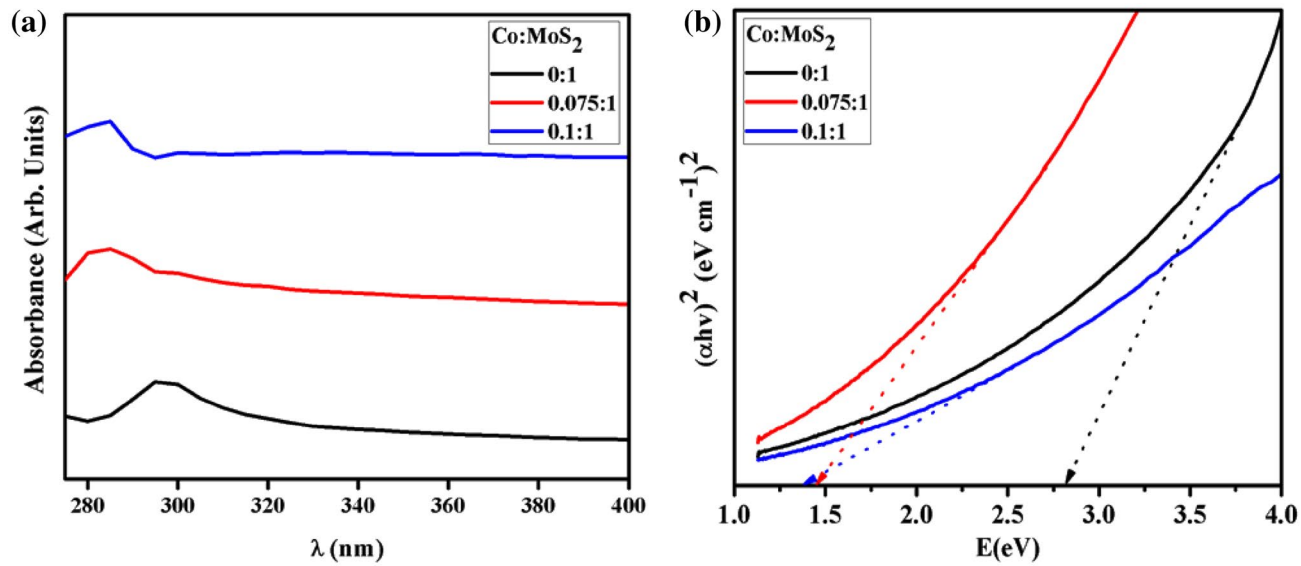

Fig. 5 **a** UV–vis spectra of various ratios of Co-doped MoS_2, **b** Bandgap analysis

lattice fringe image, which is matching up with (100) facet of hexagonal MoS_2 phase. The measured interlayer spacing d decreased gradually (0.23 and 0.22 nm) with Co is well harmonized to reported XRD results.

To find the confirmation of MoS_2 flakes, Raman analysis is necessary. Figure 7a shows Raman spectra ranging from 60 to 820 cm^{-1} of bare and doped MoS_2. Peaks around ~ 100, 176, and 730 cm^{-1} are allocated as $E^1{}_2g$–LA [M] (Wu et al. 2014), A_{1g}-LA [M] (Windom et al. 2011), and A_{1g} (M) + E_{1g} (M), respectively. Peaks found ~ 100, 180 cm^{-1}, and symmetry selection rules exclude that these peaks could be assigned to one- or two-phonon allowed modes. Furthermore, their half-widths are comparable with those of first-order allowed modes suggesting to one-phonon forbidden modes (Placidi et al. 2015). The little downshift of all peaks may be related to laser-induced heating (Wu et al. 2014). Peak at 176 cm^{-1} is assigned to longitudinal acoustic phonon mode LA(M) A1g(M)–LA(M) (Bozheyev et al. 2017). This mode feature corresponds to scattering process with a single LA(M) phonon in MoS_2 nanoparticles and thin layers. Absence of this feature may approve decent quality of synthesized samples (Gołasa 2014).

To determine the significance of the role played by Co in facilitating electron transfer, fluorescence spectra of undoped and Co-doped samples are shown in Fig. 7b. Bulk MoS_2 shows indirect BG of 1.2 eV without photoluminescence behavior, whereas exfoliated MoS_2 has direct BG ~ 1.8 eV exhibits enhanced photoluminescence caused by k-point excitons in brillouin zone. This enhancement in PL suggests quantum confinement effect on electronic structure of MoS_2. The observed PL spectra attributed to direct excitonic transition from lower to conduction band to higher spin split of valence band at K-point in Brillouin zone (Chacko et al. 2019). The most intense peak observed is located at 520 nm of MoS_2 compared to other peak. Upon doping, fluorescence intensity decreased gradually, evidence to the fact that recombination of charge was suppressed and efficiency of electron mobility was accelerated. The high excitation wavelength, PL dependent of MoS_2 corresponding to quantum confinement effects, surface states, and edge sites of MoS_2 nanostructures (Yu et al. 2017).

To further confirm the phase and thermal stability of samples, DSC-TGA measurements were performed from room temperature to 1000 °C with a ramp rate of 10 °C min^{-1} as depicted in Fig. 8a, b. Three mass loss steps located ~ 350 °C and ~ 650 °C and ~ 800 °C, suggesting to endothermic curves. The former step (~ 350 °C) weight loss around 2–3% is ascribed to removal of water as hydronium ion (H_3O^+) and latter step in the range of 350—650 °C showed a major weight loss of ~ 16% corresponding to replacement of S by O due to oxidation of MoS_2 to MoO_3 followed by sublimation of oxide (Sim et al. 2017; Wang et al. 2017; Cho et al. 2006). An abrupt weight reduction around 800 °C revealed the thermal decomposition of MoS_2 (Pandey et al. 2016). Besides, exposure at 350 °C facilitated the conversion of MoS_2 structure from 1-T phase to thermodynamically stable 2-H phase (Wang et al. 2017; Wu 2015).

Catalytic reduction of MB was examined in the presence of reducing agent $NaBH_4$ with MoS_2 nanocatalyst represented in Fig. 9a–c. Reduced capacity using $NaBH_4$ with undoped sample did not affect significantly (Fig. 9a) while catalytic efficiency of doped samples (0.1:1) indicated a quick successive reduction in MB concentration. MoS_2 shows partial reduction (44%) of dye within 40 min whereas

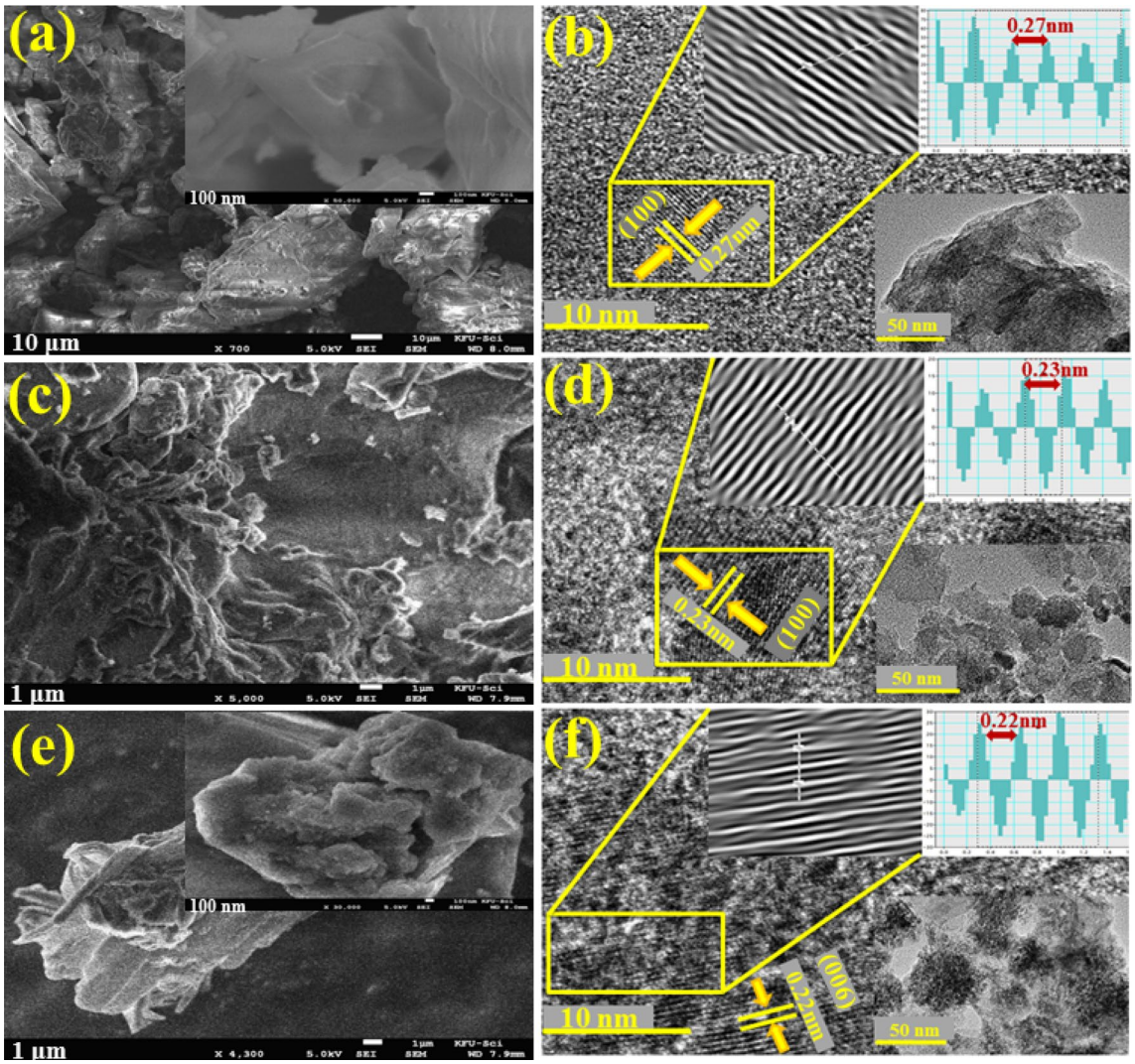

Fig. 6 FESEM and HR-TEM images of Co-doped MoS_2 **a**, **b** 0:1, **c**, **d** 0.075:1 and **e**, **f** 0.1:1

Co doped (0.075:1) degrades 47% MB in 25 min (Fig. 9b, e). Furthermore, Co doped (0.1:1) shows maximum decolorization (96%) within 3 min and MB efficiently reduces leucomethylene blue (LMB) with nanocatalyst ($NaBH_4$) at ambient temperature and maximum absorption peak of MB observed ~ 665 nm. In Fig. 9d, absorption intensity variations of MB show rapid reaction rate during definite time and that degradation increased with increasing amount of doping. Moreover, MB reduction in doped MoS_2 was merely completed at the end of reaction. On the other hand, in Fig. 9e. it can be seen that the control sample exhibits reduction of MB slowly, advising efficient catalytic property of Co–MoS_2. We believed that the doped MoS_2 is a potential nanocatalyst and can be employed in industries (Haider et al. 2019; Rafiq 2019). Using the following expression, $\ln\left(C_o/C_t\right) = kt$ where C_o is the initial concentration of dye and C_t is the concentration at time t with nanocatalyst, k is the apparent rate constant which is 0.015 min^{-1}. However a sharp increase in rate constant is observed for doped samples i.e., $k = 0.025$ min^{-1} and 1.03 min^{-1}. It is concluded that Co:MoS_2 has higher potential to degrade organic pollutant efficiently (Fig. 9d) (Arshad 2017).

Conclusion

MoS_2 nanosheets were separated via chemical exfoliation and Co (7.5 and 10 wt%) doped nanosheets were synthesized hydrothermally. XRD pattern showed the presence of doped species, and hexagonal crystal structure and an increase in crystallite sizes (16, 48.3 and 26.6) nm were found after doping without change in crystal structure. FTIR spectra confirmed bonding between S–S,

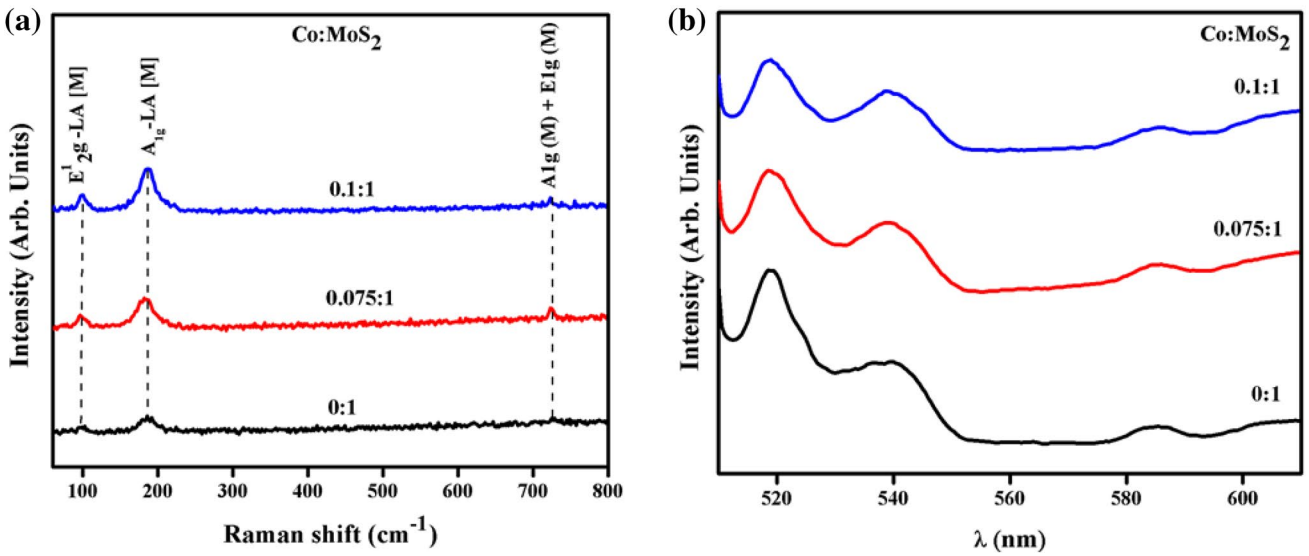

Fig. 7 **a** Raman spectra, **b** PL spectra of Co-doped MoS_2

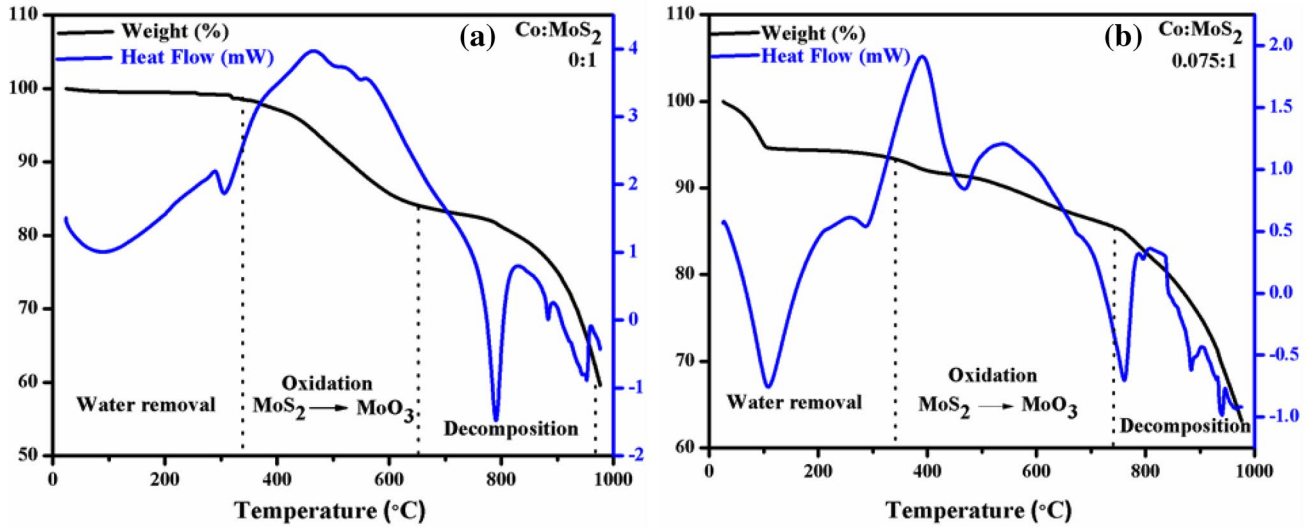

Fig. 8 **a** DSC-TGA curve of pristine MoS_2, **b** Co-doped MoS_2

characteristic peak of Mo–O around 1380 cm^{-1} and indicate that other functional groups were attached during synthesis, a gradual decrease in characteristic peak may indicate the presence of doped material. Morphological analysis displayed particle aggregation with stacking layers seems surface defects, d spacing (27, 23, 22 nm), and nanosheets were successfully visualized by HR-TEM. Co-doped nanosheets demonstrated absorbance in UV region and increase in absorption range towards longer wavelength upon doping. A decrease in BG (2.43, 1.41, and 1.35 nm) was noted which points toward the excellent potential of Co-doped nanosheets compared to pristine sample. Bulk MoS_2 successfully exfoliated to monolayer, recombination of charge was suppressed, and efficiency of electron mobility was accelerated as endorsed with PL spectra. Phase conversion, thermal decomposition, and endothermic behavior of MoS_2 was confirmed with DSC-TGA curve. Catalytic activity was studied, resulting in the conclusion that the Co-doped MoS_2 is a promising material for dye degradation (upto 96% in 3 min) and water purification. Additionally, nanosheets are cost-effective, environment friendly, and non-toxic for water desalination.

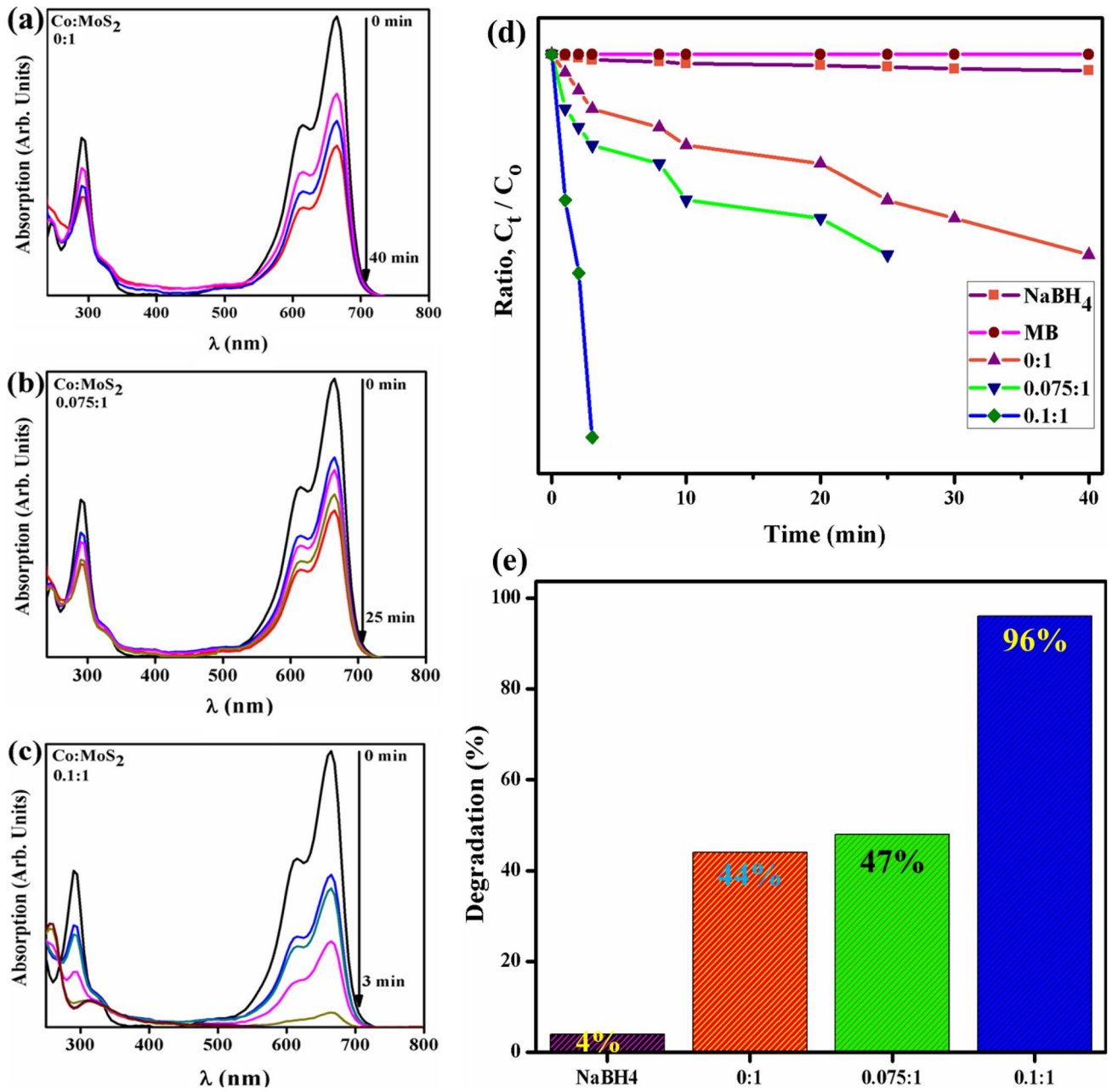

Fig. 9 **a**–**c** Time dependent UV–vis spectra of dyes reduction, **d** degradation ratio with time, **e** Comparison of degradation (%) efficiency of various ratio of Co-doped MoS_2

Acknowledgements Authors are grateful to higher education commission (HEC), Pakistan for financial support through start research group (SRGP) project number 21-1669.

Compliance with ethical standards

Conflict of interest Authors confirmed that this manuscript has no conflict of interest.

References

Arshad A et al (2017) Solar light triggered catalytic performance of graphene-CuO nanocomposite for waste water treatment. Ceram Int 43(14):10654–10660

Bozheyev F, Valiev D, Nemkayeva R (2017) Pulsed cathodoluminescence and Raman spectra of MoS_2 nanocrystals at different excitation electron energy densities and laser wavelengths. J Lumin 188:529–532

Chacko L, Rastogi PK, Aneesh PM (2019) Phase Engineering from 2H to 1T-MoS_2 for efficient ammonia PL sensor and electrocatalyst for hydrogen evolution reaction. J Electrochem Soc 166(8):H263–H271

Cho MH, Ju J, Kim SJ, Jang H (2006) Tribological properties of solid lubricants (graphite, Sb2S3, MoS_2) for automotive brake friction materials. Wear 260(7–8):855–860

Dervin S, Dionysiou DD, Pillai SC (2016) 2D nanostructures for water purification: graphene and beyond. Nanoscale 8(33):15115–15131

Feng G, Wei A, Zhao Y, Liu J (2015) Synthesis of flower-like MoS_2 nanosheets microspheres by hydrothermal method. J Mater Sci Mater Electron 26(10):8160–8166

Gołasa K et al (2014) Multiphonon resonant Raman scattering in MoS_2. Appl Phys Lett 104(9):092106

Haider A et al (2019) Enhanced bactericidal action and dye degradation of spicy roots' extract-incorporated fine-tuned metal oxide nanoparticles. Appl Nanosci. https://doi.org/10.1007/s13204-019-01188-x

Junaid M et al (2019) The study of Fe-doped CdS nanoparticle-assisted photocatalytic degradation of organic dye in wastewater. Appl Nanosci 9:1593–1602

Kumar TN, Chandrasekaran N, Lakshminarasimha K (2012) Structural and electronic modification of MoS_2 nanosheets using S-doped carbon for efficient electrocatalysis of hydrogen evolution reaction. Chem Commun 24:5

Kumar S, Sharma V, Bhattacharyya K, Krishnan V (2017) N-doped ZnO–MoS_2 binary heterojunctions: the dual role of 2D MoS_2 in the enhancement of photostability and photocatalytic activity under visible light irradiation for tetracycline degradation. Mater Chem Front 1(6):1093–1106

Kunduru KR, Nazarkovsky M, Farah S, Pawar RP, Basu A, Domb AJ (2017) "Nanotechnology for water purification: applications of nanotechnology methods in wastewater treatment", in water purification. Elsevier, Amsterdam, pp 33–74

Li J et al (2017a) Ionic liquid assisted hydrothermal synthesis of MoS_2 double-shell polyhedral cages with enhanced catalytic hydrogenation activities. RSC Adv 7(38):23523–23529

Li B et al (2017b) Preparation of monolayer MoS_2 quantum dots using temporally shaped femtosecond laser ablation of bulk MoS_2 targets in water. Sci Rep 7(1):11182

Lin H et al (2017) Rapid and highly efficient chemical exfoliation of layered MoS_2 and WS_2. J Alloy Compd 699:222–229

Liu Y, Zhao Y, Jiao L, Chen J (2014) A graphene-like MoS_2/graphene nano composite as a high performance anode for lithium ion batteries. J Mater Chem A 2(32):13109–13115

Ma L, Xu L, Xu X, Zhou X, Luo J, Zhang L (2016) Cobalt-doped edge-rich MoS_2/nitrogenated graphene composite as an electrocatalyst for hydrogen evolution reaction. Mater Sci Eng B 212:30–38

Mao J, Wang Y, Zheng Z, Deng D (2018) The rise of two-dimensional MoS_2 for catalysis. Front Phys 13(4):138118

Naz M, Haider A, Ikram M, Qureshi MZ, Ali S (2017) Green Synthesis (A indica Seed Extract) of Silver Nanoparticles (Ag-NPs), Characterization, Their Catalytic and Bactericidal Action Potential. Nanosci Nanotechnol Lett 9(11):1649–1655

Nethravathi C, Prabhu J, Lakshmipriya S, Rajamathi M (2017) Magnetic co-doped MoS_2 nanosheets for efficient catalysis of nitroarene reduction. ACS Omega 2(9):5891–5897

Oudeng G, Au M, Shi J, Wen C, Yang M (2018) One-step in situ detection of miRNA-21 expression in single cancer cells based on biofunctionalized MoS_2 nanosheets. ACS Appl Mater Interfaces 10(1):350–360

Pandey A, Dutta S, Kumar A, Raman R, Kapoor AK, Muralidhran R (2016) Structural and optical properties of bulk MoS_2 for 2D layer growth. AML 7(10):777–782

Peng H et al (2015) Co-doped MoS_2 NPs with matched energy band and low overpotential high efficiently convert CO_2 to methanol. Appl Surf Sci 353:1003–1012

Pineda-León HA et al (2018) Synthesis and characterization of molibdenum sulfide nanoparticles by a new chemical reaction formulation. Chalcogenide Lett 15:6

Placidi M et al (2015) Multiwavelength excitation Raman scattering analysis of bulk and two-dimensional MoS_2: vibrational properties of atomically thin MoS_2 layers. 2D Matter 2(3):035006

Rafiq A et al (2019) Photocatalytic and catalytic degradation of organic dye by uncapped and capped ZnS quantum dots. Mater Res Express 6(5):055801

Sim DM, Han HJ, Yim S, Choi M-J, Jeon J, Jung YS (2017) Long-term stable 2H-MoS_2 dispersion: critical role of solvent for simultaneous phase restoration and surface functionalization of liquid-exfoliated MoS_2. ACS Omega 2(8):4678–4687

Singh S et al (2019) Role of iron in the enhanced reactivity of pulverized red mud: analysis by Mössbauer spectroscopy and FTIR spectroscopy. Case Stud Constr Mater 11:e00266

Vattikuti SVP, Byon C (2015) Synthesis and characterization of molybdenum disulfide nanoflowers and nanosheets: nanotribology. J Nanomater 2015:1–11

Wahab A et al (2019) Dye degradation property of cobalt and manganese doped iron oxide nanoparticles. Appl Nanosci 9:1823–1832

Wang J et al (2016) Enhanced exfoliation effect of solid auxiliary agent on the synthesis of biofunctionalized MoS_2 using grindstone chemistry. Part Part Syst Charact 33(11):825–832

Wang D, Xiao Y, Luo X, Wu Z, Wang Y-J, Fang B (2017) Swollen Ammoniated MoS_2 with 1T/2H hybrid phases for high-rate electrochemical energy storage. ACS Sustain Chem Eng 5(3):2509–2515

Wang Z, Wu A, Colombi Ciacchi L, Wei G (2018) Recent advances in nanoporous membranes for water purification. Nanomaterial 8(2):65

Wang T et al (2018) Tulip-like MoS_2 with single sheet tapered structure anchored on N-doped graphene substrates via C–O–Mo bonds for superior sodium storage. J Mater Sci 6:18

Windom BC, Sawyer WG, Hahn DW (2011) A Raman spectroscopic study of MoS_2 and MoO_3: applications to tribological systems. Tribol Lett 42(3):301–310

Wu J-Y, Lin M-N, Wang L-D, Zhang T (2014) Photoluminescence of MoS_2 prepared by effective grinding-assisted sonication exfoliation. J Nanomater 2014:1–7

Wu Z et al (2015) Enhanced hydrogen evolution catalysis from osmotically swollen ammoniated MoS_2. J Mater Chem A 3(24):13050–13056

Wu M, Li L, Liu N, Wang D, Xue Y, Tang L (2018) Molybdenum disulfide (MoS_2) as a co-catalyst for photocatalytic degradation of organic contaminants: a review. Process Saf Environ Prot 118:40–58

Ye J, Chen W, Xu S, Yu Z, Hou S (2016) Synthesis of Co-doped MoS_2/graphene hybrids as an enhanced electrocatalyst for hydrogen evolution reaction. RSC Adv 6:10

Yi M, Zhang C (2018) The synthesis of two-dimensional MoS_2 nanosheets with enhanced tribological properties as oil additives. RSC Adv 8(17):9564–9573

Yin Z et al (2014) Au nanoparticle-modified MoS_2 nanosheet-based photoelectrochemical cells for water splitting. Small 10(17):3537–3543

Yu H, Xu J, Guo H, Li Y, Liu Z, Jin Z (2017) Synergistic effect of rare earth metal Sm oxides and Co_{1-x} S on sheet structure MoS_2 for photocatalytic hydrogen evolution. RSC Adv 7(89):56417–56425

Zeng X, Niu L, Song L, Wang X, Shi X, Yan J (2015) Effect of polymer addition on the structure and hydrogen evolution reaction property of nanoflower-like molybdenum disulfide. Metals 5(4):1829–1844

Zhang X et al (2018) Photocatalytic activity of 3D flower-like MoS_2 hemispheres. Mater Res Bull 100:249–253

Zhiming M (2013) MoS_2. Springer, Berlin Heidelberg, New York